© 2016. Published by The Company of Biologists Ltd | Development (2016) 143, 4173-4181 doi:10.1242/dev.141861

RESEARCH ARTICLE

A network of conserved formins, regulated by the guanine exchange factor EXC-5 and the GTPase CDC-42, modulates tubulogenesis *in vivo*

Daniel D. Shaye[1,2,3,*] and Iva Greenwald[1,2]

ABSTRACT

The *C. elegans* excretory cell (EC) is a powerful model for tubulogenesis, a conserved process that requires precise cytoskeletal regulation. EXC-6, an ortholog of the disease-associated formin INF2, coordinates cell outgrowth and lumen formation during EC tubulogenesis by regulating F-actin at the tip of the growing canal and the dynamics of basolateral microtubules. EXC-6 functions in parallel with EXC-5/FGD, a predicted activator of the Rho GTPase Cdc42. Here, we identify the parallel pathway: EXC-5 functions through CDC-42 to regulate two other formins: INFT-2, another INF2 ortholog, and CYK-1, the sole ortholog of the mammalian diaphanous (mDia) family of formins. We show that INFT-2 promotes F-actin accumulation in the EC, and that CYK-1 inhibits INFT-2 to regulate F-actin levels and EXC-6-promoted outgrowth. As INF2 and mDia physically interact and cross-regulate in cultured cells, our work indicates that a conserved EXC-5–CDC-42 pathway modulates this regulatory interaction and that it is functionally important *in vivo* during tubulogenesis.

KEY WORDS: FGD, Cdc42, INF2, Diaphanous, Tubulogenesis, *C. elegans*

INTRODUCTION

Biological tube formation and maintenance (tubulogenesis) is a conserved process that requires precise cytoskeletal regulation and is essential for organogenesis in all metazoans (Iruela-Arispe and Beitel, 2013). The *Caenorhabditis elegans* excretory cell (EC) is a single-celled epithelial tube in which the cell's apical domain abuts the lumen and the basolateral domain is the outer edge. The EC is a 'seamless' tube that does not have adherens or tight junctions along its length; instead, it has a junction where it connects to its neighboring cell. Such seamless tubes are found in vertebrate vascular systems, as well as in invertebrate organs and glia (Sundaram and Cohen, 2016).

The EC is a tractable model to study the genetic control of tubulogenesis (Sundaram and Buechner, 2016). Several conserved regulators of tubulogenesis were identified in a pioneering screen for mutations that resulted in cystic excretory cell canals (Buechner et al., 1999). One of these, *exc-6*, encodes an ortholog of the formin INF2 (Shaye and Greenwald, 2015). *INF2* is mutated in autosomal dominant focal segmental glomerulosclerosis (FSGS), a kidney disease, and Charcot–Marie–Tooth (CMT) neuropathy with associated FSGS (Boyer et al., 2011; Brown et al., 2010). Disease-causing mutations that constitutively activate human INF2 can substitute for EXC-6 in EC tubulogenesis (Shaye and Greenwald, 2015), further underscoring the conservation of function. Our analysis suggested that EXC-6 regulates basolateral microtubule dynamics, and organizes actin and microtubule cytoskeletons at the leading edge to coordinate basolateral and apical outgrowth during EC tubulogenesis (Shaye and Greenwald, 2015). However, despite the well-characterized role of formins as canonical actin-polymerizing factors (Breitsprecher and Goode, 2013), animals carrying an *exc-6* null allele [hereafter null alleles will be denoted as (*0*)] did not display overt defects in F-actin levels in the EC. We therefore sought to identify actin-polymerizing factors that promote tubulogenesis in the EC, and to ascertain how they are regulated.

Members of the Rho/Rac/Cdc42 GTPase family are well-known actin regulators that function via a myriad of downstream effectors, including formins (Kühn and Geyer, 2014). There is some evidence that the *C. elegans* ortholog of Cdc42 plays a role in EC tubulogenesis. First, either loss or excessive activity of EXC-5, an ortholog of the faciogenital dysplasia-associated (FGD) family of guanine exchange factors (GEFs) that specifically activate Cdc42 in biochemical and cell culture assays (Hayakawa et al., 2008; Huber et al., 2008; Kurogane et al., 2012; Miyamoto et al., 2003; Steenblock et al., 2014; Umikawa et al., 1999; Zheng et al., 1996), causes defects in EC tubulogenesis (Buechner et al., 1999; Gao et al., 2001; Mattingly and Buechner, 2011; Suzuki et al., 2001). Second, reduced *cdc-42* activity causes mild EC phenotypes associated with defects in endocytic trafficking (Lant et al., 2015), and overexpression of wild-type, dominant-negative, or activated CDC-42 also affect EC tubulogenesis (Mattingly and Buechner, 2011). However, whether CDC-42 regulates actin in the EC and which actin-polymerizing factors may be involved has been unknown.

Here, we demonstrate that EXC-5 acts through CDC-42 to regulate two conserved formins in EC tubulogenesis: INFT-2, a second INF2 ortholog (and thus an EXC-6 paralog), and CYK-1, the sole ortholog of the mammalian diaphanous (mDia) family of formins. Cell culture and *in vitro* analysis suggest that human INF2 binds to mDia and inhibits its ability to polymerize actin (Sun et al., 2013, 2011). Our work demonstrates that the reciprocal regulatory interaction occurs *in vivo*: CYK-1 negatively regulates the actin-polymerizing function of INFT-2, and this plays a role in regulating F-actin levels and EXC-6-promoted EC outgrowth. Our results suggest that a conserved network of formins, regulated by EXC-5 and CDC-42, regulates tubulogenesis *in vivo*, and we propose that

[1]Department of Biological Sciences, Columbia University, New York, NY 10027, USA. [2]Department of Biochemistry and Molecular Biophysics, Columbia University, New York, NY 10032, USA. [3]Department of Physiology and Biophysics, University of Illinois at Chicago, Chicago, IL 60612, USA.

*Author for correspondence (shaye@uic.edu)

D.D.S., 0000-0002-3962-6903

Received 6 July 2016; Accepted 20 September 2016

Development (2016) 143, 4173-4181 doi:10.1242/dev.141861

similar relationships might operate in mammalian development and disease.

RESULTS

An EXC-5–CDC-42 pathway functions in parallel with EXC-6 to promote EC outgrowth

During embryogenesis, the EC generates two processes, each containing a growing intracellular lumen, that first grow dorsally from the left and right sides of the EC body and then split to form four canals; two grow anteriorly and two grow posteriorly. During the first larval stage, the canals actively grow until they span almost the entire length of the animal: the anterior canals terminate prior to reaching the buccal cavity, and the posterior canals typically terminate at or near the rectum. Thereafter, the canals continue to grow passively to keep up with the lengthening body (Sundaram and Buechner, 2016; Fig. 1A,G; Fig. 3A,B,D).

We previously showed that EXC-6 is required for canal outgrowth, and that the canals of *exc-5(0); exc-6(0)* double mutants are shorter than in either single mutant, indicating that EXC-5 functions in a pathway parallel with EXC-6 (Shaye and Greenwald, 2015; see also Fig. 1B-D,G). To identify this pathway, we investigated whether CDC-42, the putative target of EXC-5, functions in EC outgrowth. We first tested the effect of zygotic loss of CDC-42, denoted *cdc-42(0*)*, as they must be derived from heterozygous mothers owing to maternal-effect lethality of the null allele. We found that *cdc-42(0*)* animals have normal-length canals (Fig. 1E,G) rather than a phenotype similar to *exc-5(0)*, perhaps because of a maternal contribution of *cdc-42(+)*. However, the canals of *cdc-42(0*); exc-6(0)* are short compared with *exc-6(0)* mutants (Fig. 1F,G) suggesting that, like EXC-5, CDC-42 functions in parallel with EXC-6 to regulate EC outgrowth.

To assess whether CDC-42 functions downstream of EXC-5, we investigated whether *cdc-42(0*)* can suppress the defects associated with *exc-5* overexpression. Both EXC-5 loss and overexpression cause canal shortening; however, the underlying defects are distinct and opposite, underscoring the importance of coordinating apical lumen growth with basolateral cell outgrowth. In *exc-5(0)* there are large cystic regions associated with fragmented apical cytoskeleton and reduced F-actin (Buechner et al., 1999; Shaye and Greenwald,

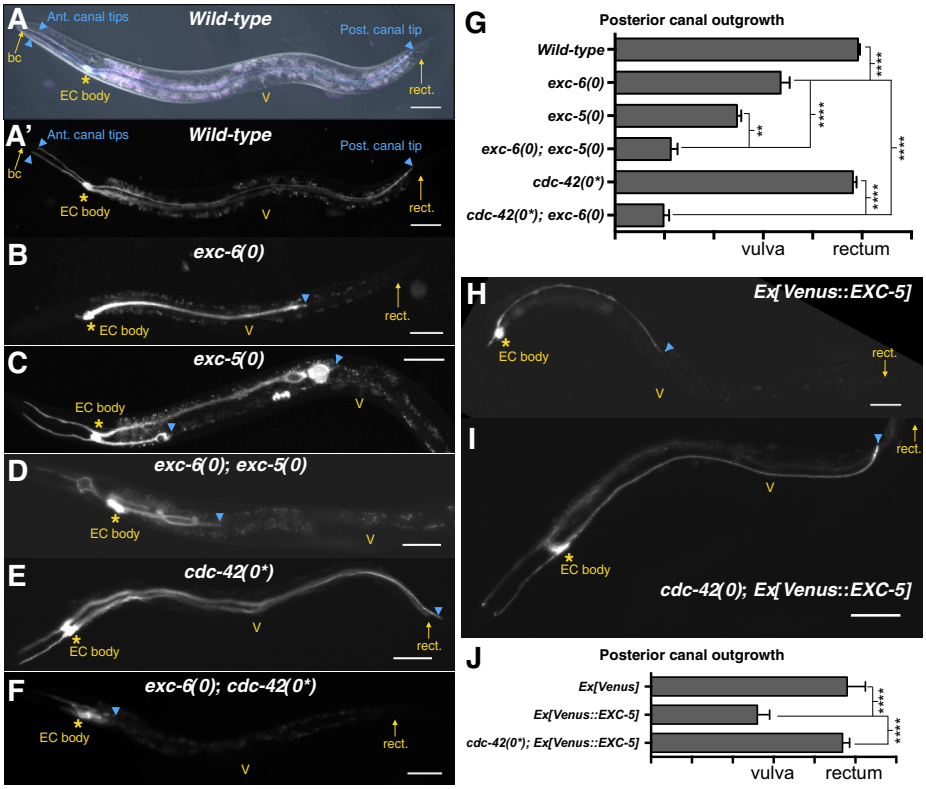

Fig. 1. An EXC-5–CDC-42 pathway regulates EC outgrowth in parallel with EXC-6. For full genotypes, here and in all subsequent figures, see Table S1. (A,A′) An otherwise wild-type hermaphrodite carrying *arIs198*, a transgene that expresses cytoplasmic cyan fluorescent protein (CFP) and LifeAct::TagRFP in the EC (Shaye and Greenwald, 2015). This same transgene is visualized in all photomicrographs in this figure. The animal shown in A was visualized using differential interference contrast, with CFP and TagRFP fluorescence (cyan/magenta) superimposed. Fluorescence alone was visualized in A′, and in subsequent photomicrographs in this figure. The buccal cavity (bc), vulva (V) and rectum (rect.) are highlighted as landmarks to gauge extent of EC anterior (ant.) and posterior (post.) canal outgrowth (cyan arrowheads). Asterisks mark the position of the EC body. (B) *exc-6(0)* hermaphrodites exhibit EC canal shortening. (C) *exc-5(0)* hermaphrodites exhibit EC canal shortening and cysts, as previously reported (Buechner et al., 1999; Gao et al., 2001; Suzuki et al., 2001). (D) *exc-6(0); exc-5(0)* double mutants exhibit synergistic canal shortening. (E) *cdc-42(0*)* mutants lack zygotic *cdc-42* activity and do not exhibit obvious canal shortening. (F) *cdc-42(0*); exc-6(0)* double mutants exhibit synergistic canal shortening. (G) Quantification of posterior canal outgrowth as shown in A-F. For each genotype, $n \geq 54$ canal arms were scored. Here, and in all subsequent graphs, the bars represent the mean, error bars represent the 95% confidence interval, and significance was calculated with Prism (GraphPad Software) by performing a non-parametric ANOVA (Kruskal–Wallis test) using Dunn's correction for multiple comparisons. *$P \leq 0.05$, **$P \leq 0.01$, ***$P \leq 0.001$, ****$P \leq 0.0001$. (H) Hermaphrodites carrying *arEx2360*[*glt-3*p::Venus::EXC-5] have shortened canals, as previously described for *exc-5* overexpression (Mattingly and Buechner, 2011; Suzuki et al., 2001). (I) *cdc-42(0*)* suppresses the canal-shortening phenotype caused by Venus::EXC-5. (J) Quantification of the outgrowth defect caused by Venus::EXC-5, and suppression by *cdc-42(0*)*. For each genotype, $n \geq 60$ canal arms were scored. Scale bars: 50 µm.

Development (2016) 143, 4173-4181 doi:10.1242/dev.141861

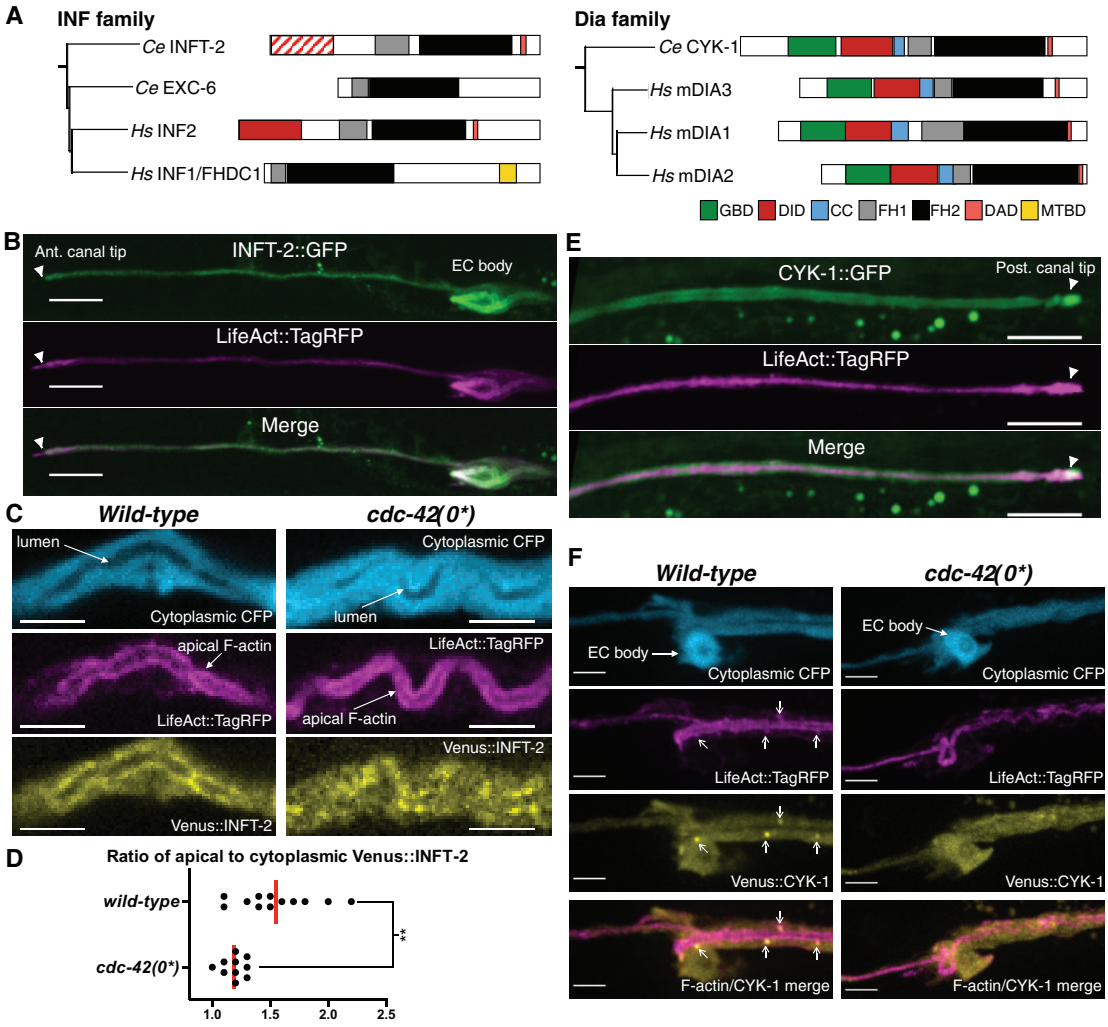

Fig. 2. INFT-2 and CYK-1 are expressed in the EC and regulated by CDC-42. (A) Evolutionary relationship (based on FH2 domain comparison) and schematics of *C. elegans* (*Ce*) and human (*Hs*) INF2 and mDia formins [mDia1-3 (DIAPH1-3), see Mi-Mi et al., 2012; Fig. S1]. GBD, G protein-binding domain; DID, diaphanous inhibitory domain; CC, coiled-coil region; FH1, formin homology 1; FH2, formin homology 2; DAD, diaphanous autoregulatory domain; MTBD, microtubule-binding domain found specifically in INF1/FHDC1 (Young et al., 2008). Note that the INFT-2 N-terminus is diverged, and only shows a 'partial' DID (hatched lines) (Mi-Mi, et al., 2012; Fig. S2). (B) INFT-2::GFP from a fosmid (carried on the transgene *arEx2348*; see supplementary Materials and Methods) is expressed in the EC and colocalizes with apical and tip LifeAct::TagRFP. (C,D) Venus::INFT-2 (expressed from the transgene *arEx2406*; see Tables S1,S2) colocalizes with apical F-actin in wild type, but this colocalization is reduced in zygotic *cdc-42(0*)* mutants. (D) Quantification of apical accumulation of Venus::INFT-2. Each point represents an individual transgenic animal. (E) CYK-1::GFP from a fosmid (carried on the transgene *arEx2357*; see Tables S1,S2) is expressed in the EC, and is found in the cytoplasm along the canals and at the leading edge tip. (F) Venus::CYK-1 (expressed from the transgene *arEx2410*; see Tables S1,S2) is seen in the cytoplasm and in distinct punctate structures that also accumulate LifeAct::TagRFP (see Movies 1 and 2). Punctate Venus::CYK-1 is lost in *cdc-42(0*)* mutants (see Movie 3). Arrows indicate punctate Venus::CYK-1 structures that accumulate LifeAct::TagRFP. Scale bars: 10 µm (B,E); 5 µm (C,F).

2015; Suzuki et al., 2001), whereas EXC-5 overexpression causes excessive and convoluted apical lumen to form (Mattingly and Buechner, 2011; Suzuki et al., 2001). We expressed Venus::EXC-5 specifically in the EC (*Ex[Venus::EXC-5]*; see supplementary Materials and Methods), causing the distinctive EC canal shortening defect expected (Fig. 1H,J). This defect was completely suppressed by *cdc-42(0*)* (Fig. 1I,J), indicating that CDC-42 acts downstream of EXC-5 in the EC.

The formins INFT-2 and CYK-1 are expressed in the EC and regulated by CDC-42

Formins are well-known effectors of the Rho/Rac/Cdc42 GTPase family (Kühn and Geyer, 2014). Canonical formins have several conserved domains (Fig. 2A), including two 'formin homology' domains (FH1 and FH2) that promote F-actin polymerization. FH domains are sometimes flanked by an N-terminal 'diaphanous inhibitory domain' (DID) and a C-terminal 'diaphanous autoregulatory domain' (DAD), which associate intra-molecularly to cause autoinhibition. Binding of activated Rho/Rac/Cdc42 GTPases to N-terminal sequences, such as the DID or other defined G protein-binding domains (GBDs), interferes with auto-inhibition, leading to formin activation (Breitsprecher and Goode, 2013).

Our finding that CDC-42 acts downstream of EXC-5, and in parallel with EXC-6, in EC tubulogenesis suggested that GBD- and/or DID-containing formins, which can be potentially regulated by CDC-42, might be actin-polymerizing factors in the EC. Two such formins were particularly compelling candidates (Fig. 2A): INFT-2, the second *C. elegans* INF2 ortholog and thus an EXC-6 paralog, because mammalian INF2 is regulated by Cdc42 via its DID

Development (2016) 143, 4173-4181 doi:10.1242/dev.141861

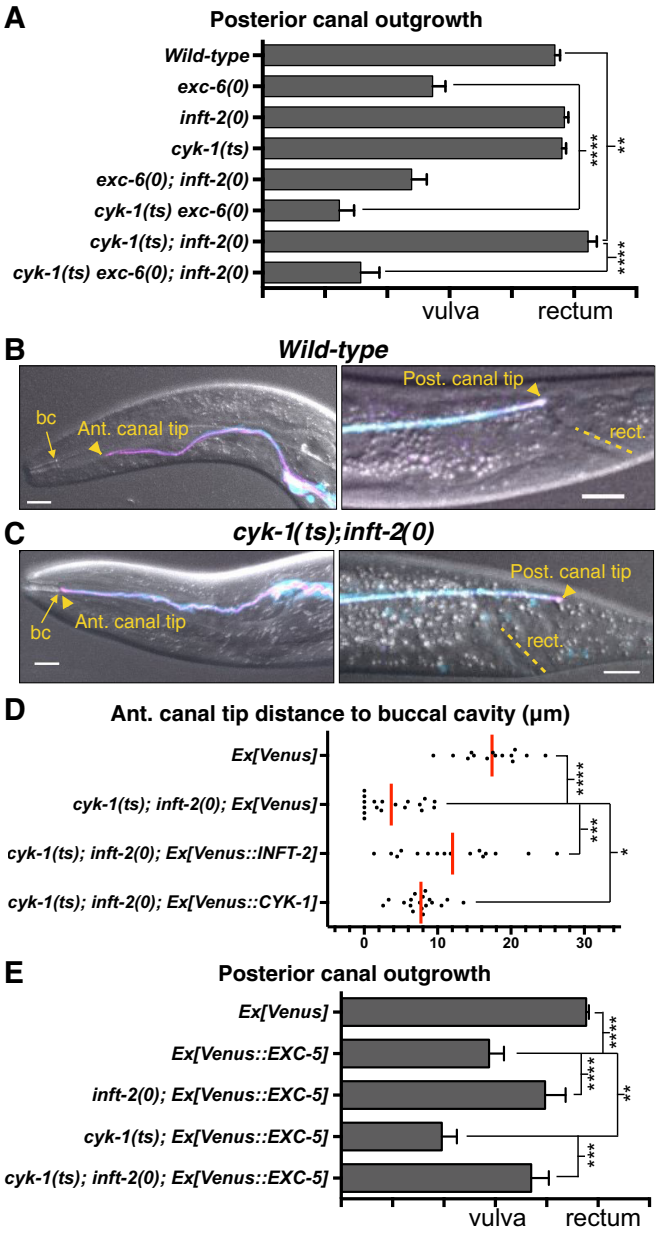

Fig. 3. INFT-2 and CYK-1 regulate EC outgrowth. (A) Genetic interactions between *exc-6*, *inft-2* and *cyk-1*. Analysis of all genotypes shown in this figure (see Table S1) was performed by applying a temperature shift to achieve strong reduction of CYK-1 function in *cyk-1(ts)* mutants, as described in the main text and in Materials and Methods. For each genotype, $n \geq 76$ canal arms were scored. Concomitant loss of EXC-6 and CYK-1 causes a strong synergistic effect, similar to that seen in *exc-6(0); exc-5(0)* and *cdc-42(0*); exc-6(0)* double mutants (Fig. 1G). Single *inft-2(0)* and *cyk-1(ts)* mutants do not display outgrowth defects, but the *cyk-1(ts); inft-2(0)* double displays significant overgrowth that is overcome by loss of *exc-6*. (B,C) In a wild-type background (B), the anterior (Ant.) canal terminates well before reaching the buccal cavity (bc) and the posterior (Post.) canal terminates at the rectum (rect.) whereas in *cyk-1(ts); inft-2(0)* hermaphrodites (C) there is significant overgrowth. (D) Quantification of anterior canal overgrowth in *cyk-1(ts); inft-2(0)* double mutants, and rescue by Venus-tagged INFT-2 (*arEx2406*) and CYK-1 (*arEx2410*). Each dot represents the distance (in µm) from the tip of an anterior canal arm to the buccal cavity, with the red bar representing the mean of all measurements. (E) Loss of INFT-2 suppresses, whereas loss of CYK-1 exacerbates, the defects caused by Venus::EXC-5 overexpression (*arEx2360*). In the triple combination, the outgrowth phenotype is not significantly different from that of *inft-2(0); Ex[Venus::EXC-5]* double mutants. For each genotype, $n \geq 60$ canal arms were scored. Scale bars: 10 µm.

(Madrid et al., 2010); and CYK-1, the sole ortholog of mDia (Mi-Mi et al., 2012), because a direct interaction between INF2 and mDia, modulated by Cdc42, had been described and found to regulate F-actin in cell culture (Sun et al., 2013, 2011).

In considering the relationship of the two *C. elegans* paralogs with INF2, we note that phylogenetic analysis clearly places INFT-2 in the same family as human INF2 (Mi-Mi et al., 2012; Fig. S1), and that EXC-6 is more closely related to INF2, whether the analysis is based on the FH2 domain, which is generally the basis of such analyses (Chalkia et al., 2008; Liu et al., 2010; Mi-Mi et al., 2012), or the entire protein (Mi-Mi et al., 2012; Fig. S1). Previous sequence analysis of the N terminus of *C. elegans* INFT-2 showed that it is diverged from mammalian formins even though it contains a predicted partial DID (Mi-Mi et al., 2012; Fig. S2). We find that this partial DID retains some residues important for intra-molecular DID-DAD interactions, as well as some of the residues that are mutated in human disease, including those required for the INF2 and mDia inter-molecular interaction (Fig. S2).

We found that INFT-2 and CYK-1 are expressed in the EC using translational green fluorescent protein (GFP) fusions expressed from fosmids (Sarov et al., 2012). INFT-2::GFP colocalizes with LifeAct::TagRFP, an *in vivo* marker for F-actin (Riedl et al., 2008), which is enriched along the lumen-lining apical membrane and at the leading edge (Fig. 2B). We note that although a recent report suggests that LifeAct may affect actin dynamics (Courtemanche et al., 2016), we find that several LifeAct::TagRFP-expressing transgenes do not cause any EC phenotypes (Shaye and Greenwald, 2015), and LifeAct remains a reliable marker for measuring total F-actin (Courtemanche et al., 2016; see also below). Venus::INFT-2, shown to function in the EC as described below, also colocalizes with F-actin, and colocalization was lost in *cdc-42(0*)* mutants (Fig. 2C,D), suggesting that CDC-42 regulates INFT-2.

CYK-1::GFP is found in the cytoplasm and in punctate structures in many tissues (not shown). In the EC, it accumulates at the actin-rich leading edge and in the cytoplasm (Fig. 2E). Localization of a functional (see below) Venus::CYK-1 specifically expressed in the EC displays similar accumulation, with visible punctate structures that also accumulate LifeAct::TagRFP (Fig. 2F, arrows; Movies 1 and 2). Punctate accumulation of Venus::CYK-1 was greatly reduced in *cdc-42(0*)* mutants (Fig. 2F; Movie 3), suggesting that CYK-1 is also regulated by CDC-42.

INFT-2 and CYK-1 function in the EC as regulators of outgrowth

To assess roles for CYK-1 and INFT-2 in EC tubulogenesis, we analyzed mutants affecting these formins. A predicted *inft-2(0)* allele is viable (Mi-Mi et al., 2012) and does not cause overt EC defects (Fig. 3A). We did not observe further shortening of the EC canals in *exc-6(0); inft-2(0)* double mutants compared with the *exc-6(0)* mutant (Fig. 3A), suggesting that the two INF2 paralogs in *C. elegans* are not functionally redundant for this role. Although the distorted morphology of the EC, including the presence of multiple lumens, resulting from *exc-6(0)* precluded more detailed analysis of this double mutant, genetic interactions between *inft-2* and *cyk-1*, and quantitative analysis of F-actin levels, suggest that INFT-2 regulates outgrowth and F-actin accumulation in the EC (see below).

A predicted *cyk-1(0)* allele causes maternal-effect sterility: homozygotes derived from heterozygous mothers survive to adulthood, but are sterile (Mi-Mi et al., 2012). Such zygotic *cyk-1(0*)* mutants do not display EC defects (not shown). However, *cyk-1(0*)* combined with either *exc-6(0)* or *inft-2(0)* (see Table S1) causes synthetic embryonic lethality, suggesting that CYK-1 and

Development (2016) 143, 4173-4181 doi:10.1242/dev.141861

the INF2 paralogs may play redundant essential roles during embryonic development. To bypass the synthetic lethality of genetic combinations with *cyk-1(0)*, we used a recessive, fast-acting and strong temperature-sensitive (*ts*) allele of *cyk-1* (Davies et al., 2014; Jordan et al., 2016). We shifted *cyk-1(ts)* mutant embryos to the non-permissive temperature and maintained them at the restrictive temperature until they were L4 larvae or young adults, so that EC development occurred primarily or exclusively at the restrictive temperature (see Materials and Methods). This protocol was followed for both single and compound mutants. We note that by using this protocol we are interfering with CYK-1 function both during the embryonic/early larval 'active' EC outgrowth phase, and during the later larval 'passive' outgrowth phase (Sundaram and Buechner, 2016). Therefore, any defects seen may reflect disruption of either, or both, these stages of EC outgrowth. Although single *cyk-1(ts)* mutants did not display any obvious EC defects, in *exc-6 (0) cyk-1(ts)* double mutants, there is strong enhancement of the *exc-6(0)* canal-shortening phenotype (Fig. 3A), similar to that seen in *exc-6(0); exc-5(0)* and *cdc-42(0*); exc-6(0)* double mutants (Fig. 1G). This observation is consistent with CYK-1 functioning in the same pathway as EXC-5 and CDC-42, in parallel with EXC-6, to promote EC outgrowth.

We examined *cyk-1(ts); inft-2(0)* double mutants and saw overgrowth of both anterior and posterior canals (Fig. 3A,C,D). This observation was surprising, because *exc-6(0); cyk-1(ts)* double mutants had shorter canals, suggesting that CYK-1 promotes outgrowth, and because *exc-6(0); inft-2(0)* double mutants had the same phenotype as the *exc-6(0)* single mutant, which initially suggested that INFT-2 does not play a role in outgrowth. Instead, the extended canals of *cyk-1(ts); inft-2(0)* double mutants suggest that CYK-1 and INFT-2 have redundant inhibitory roles in EXC-6-promoted outgrowth. This conclusion is supported by the observation that the *cyk-1(ts); inft-2(0); exc-6(0)* triple mutant does not display overgrowth (Fig. 3A). Moreover, *cyk-1(ts) exc-6(0)* double mutants, which show synergistic effects for EC outgrowth, still continue to show the cystic and multiple-lumen phenotypes of the *exc-6(0)* single mutant (Fig. S3). This epistatic relationship is consistent with CYK-1 acting upstream of EXC-6, directly or indirectly, to modulate its function.

The inhibitory role of INFT-2, revealed when *inft-2(0)* is combined with *cyk-1(ts)*, is the only role we have detected in EC outgrowth for this formin. This further underscores the lack of functional redundancy beween INFT-2 and EXC-6, which only plays a positive role. Detection of both positive and negative roles for CYK-1 in outgrowth, revealed in *cyk-1(ts)* double mutants with *exc-6(0)* and *inft-2(0)*, respectively, suggests that CYK-1 may have multiple targets in EC tubulogenesis. We infer that reduced CYK-1 activity creates a sensitized background, where the resulting phenotype (EC overgrowth or reduced outgrowth) depends on whether loss of a positive or a negative outgrowth regulator is combined with *cyk-1(ts)*.

The canal-overgrowth phenotype of the *cyk-1(ts); inft-2(0)* double mutant allowed us to test both EC-autonomy and functionality of the Venus-tagged proteins studied in Fig. 2. Transgenes expressing either Venus::INFT-2 or Venus::CYK-1 in the EC rescued the synthetic overgrowth phenotype of *cyk-1(ts); inft-2(0)* double mutants (Fig. 3D), indicating that these formins act in the EC and that the Venus-tagged proteins used to assess localization are functional. Taken together, these results suggest the existence of a functional network involving all three formins (the two INF2 orthologs, EXC-6 and INFT-2, and CYK-1) in the EC that regulates outgrowth during tubulogenesis.

The activities of CYK-1 and INFT-2 are regulated by the EXC-5–CDC-42 pathway

To determine whether the outgrowth-modulating activities of CYK-1 and INFT-2 are regulated by the EXC-5–CDC-42 pathway, we analyzed how loss of these formins modifies the phenotype caused by overexpressing Venus::EXC-5 (Fig. 3E). We found that *inft-2(0)* suppressed the EC outgrowth phenotype caused by *Ex[Venus::EXC-5]*, as well as other phenotypes (Fig. S4), suggesting that INFT-2 functions downstream of the EXC-5–CDC-42 pathway. In both this genetic test and in the double *cyk-1(ts); inft-2(0)* mutant, the genetic behavior of *inft-2* is consistent with a role as a negative regulator of EC outgrowth in this pathway.

By contrast, the *cyk-1(ts)* mutation enhanced the EC outgrowth phenotype caused by *Ex[Venus::EXC-5]* (Fig. 3E) as well as other phenotypes (Fig. S4), consistent with the hypothesis that *cyk-1* is a positive regulator of outgrowth suggested by the strong enhancement of the *exc-6(0)* outgrowth defect in *cyk-1(ts)*. CYK-1 might act by inhibiting a negative regulator activated by the EXC-5–CDC-42 pathway, the most obvious candidate being INFT-2. Our genetic, F-actin, and Venus::INFT-2 accumulation data below support this hypothesis.

Finally, we considered the genetic interactions between *cyk-1* and *inft-2* in relation to an over-activated EXC-5–CDC-42 pathway. When we examined the effect of simultaneous reduction of both formins on the canal phenotypes caused by *Ex[Venus::EXC-5]*, we found that canal shortening (Fig. 3E), and other EC phenotypes (Fig. S4), were suppressed, as in the *inft-2(0)* single mutant. Essentially, *inft-2(0)* is epistatic to *cyk-1(ts)* in these genetic assays, consistent with a function for INFT-2 downstream of CYK-1.

CYK-1 regulates *inft-2*-dependent F-actin levels and INFT-2 accumulation

Formins are canonical actin-polymerizing factors (Breitsprecher and Goode, 2013), so we investigated whether the EXC-5–CDC-42 pathway, and its downstream effectors, the formins INFT-2 and CYK-1, regulate F-actin in the EC by quantifying LifeAct::TagRFP fluorescence (Riedl et al., 2008) using *in vivo* spinning disk confocal microscopy (Fig. 4A,B; Materials and Methods). We note that although recent evidence suggests that LifeAct may affect actin polymerization kinetics, it remains a reliable marker for measuring the total number of polymerized actin molecules (Courtemanche et al., 2016).

F-actin is significantly reduced in *exc-5(0)* compared with wild type (Fig. 4B, green and blue, respectively), similar to the reduction in F-actin seen in *inft-2(0)* (Fig. 4B, yellow), suggesting that INFT-2 promotes F-actin accumulation in the EC. Conversely, F-actin is significantly increased in *cyk-1(ts)* mutants, suggesting that this formin inhibits F-actin accumulation in the EC (Fig. 4B, red), consistent with our genetic observations that INFT-2 and CYK-1 can play opposing roles in EC outgrowth. Finally, the increased F-actin seen in *cyk-1(ts)* is dependent on INFT-2, as the *cyk-1(ts); inft-2(0)* double mutant displays reduced F-actin (Fig. 4B, orange) compared with *cyk-1(ts)* alone. To determine whether CYK-1 regulates INFT-2 by modulating its levels and/or localization, we crossed the Venus::INFT-2 reporter into *cyk-1(ts)*. We found a significant increase in Venus::INFT-2 accumulation at the apical membrane (Fig. 4C,D), suggesting that CYK-1 is a negative regulator of INFT-2 levels and/or accumulation. Together, the genetic and F-actin accumulation analyses show that INFT-2 is an actin-polymerizing factor in the EC, and that its activity is inhibited by CYK-1.

Development (2016) 143, 4173-4181 doi:10.1242/dev.141861

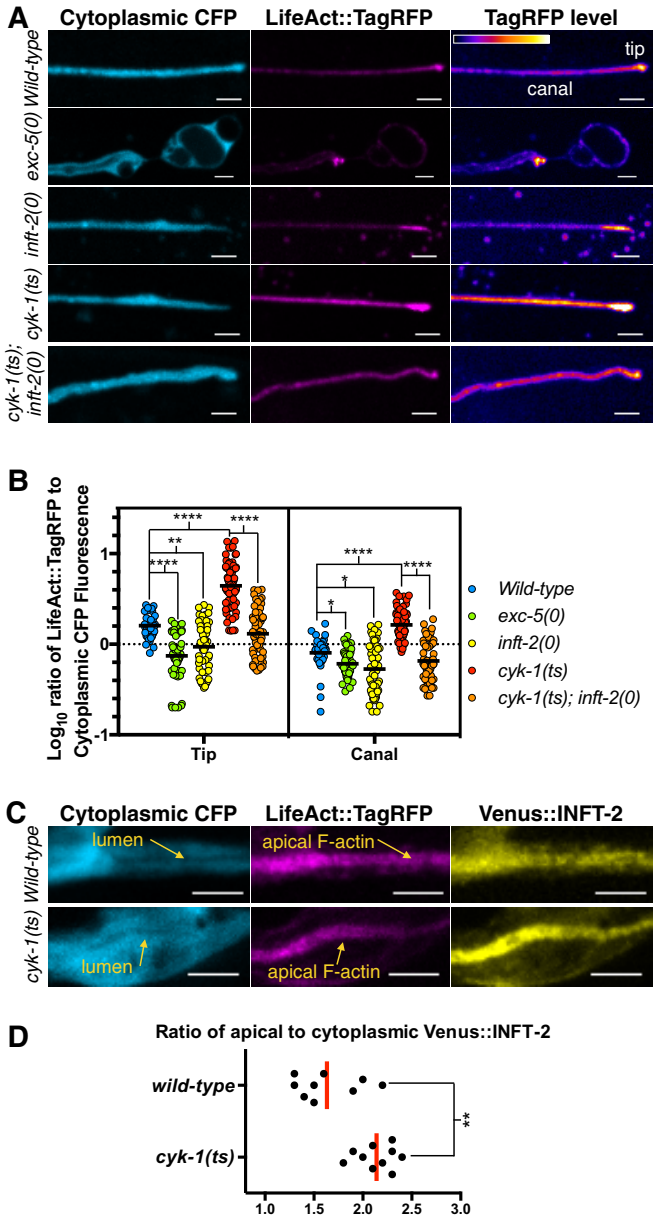

Fig. 4. CYK-1 regulates INFT-2 accumulation and *inft-2*-dependent F-actin in the EC. For details on image acquisition and analysis, see supplementary Materials and Methods. (A) Representative confocal projections of posterior EC canals from different genotypes showing cytoplasmic CFP and LifeAct::TagRFP (expressed from transgene *arIs198*), as well as conversion of TagRFP fluorescence levels to a gradient where no expression is represented by black, and highest levels of expression are denoted in white. (B) Quantification of the ratio of LifeAct::TagRFP to cytoplasmic CFP fluorescence as a measure of LifeAct::TagRFP levels. In the scatter graph, each point represents a measurement carried out on a single 0.5 µm confocal *z*-section to prevent confounding additive effects from projections. For each genotype, ≥10 canals were analyzed, with three to seven *z*-sections measured for each (depending on canal topology), to ensure measurement of entire width of lumen and tip. The 'tip' measurements were performed on an area, typically ~5 µm^2, at the end of posterior EC canals. The 'canal' measurements were performed on a similar-sized area at least 5 µm away from the tip, to avoid measuring regions that might belong to the leading edge. Black horizontal lines represent the mean values. (C) Animals carrying Venus::INFT-2 (expressed from *arEx2406*) in wild-type and *cyk-1(ts)* backgrounds were temperature shifted (see Materials and Methods) in parallel, and apical Venus::INFT-2 accumulation increased when CYK-1 function was reduced. (D) Quantification of apical accumulation of Venus::INFT-2. Each point represents an individual transgenic animal. Scale bars: 5 µm.

DISCUSSION

Unicellular tube formation requires coordinated growth of apical and basolateral membranes. During EC tubulogenesis, EXC-6, one of two *C. elegans* orthologs of human INF2, promotes outgrowth by regulating basolateral microtubule dynamics and by organizing the F-actin/microtubule-rich leading edge structure, which coordinates the growth of both membranes (Shaye and Greenwald, 2015). Here, we have defined a parallel genetic pathway headed by *exc-5*, which encodes the ortholog of human FGD, an established activator of the Rho GTPase Cdc42. We show that during EC tubulogenesis, EXC-5 acts through CDC-42 to regulate the activity of two other formins: INFT-2, the other *C. elegans* INF2 ortholog, and CYK-1, the sole ortholog of the mammalian diaphanous (mDia) family of formins.

We have also examined the accumulation of fluorescently tagged proteins in different mutant backgrounds to probe the roles of these genes from a cell biological perspective. We thereby show that INFT-2 promotes apical and leading edge F-actin accumulation. We also show that CYK-1 negatively regulates INFT-2 apical localization, inhibits the ability of INFT-2 to promote F-actin accumulation, and may act via a distinct target to inhibit basolateral outgrowth. As INF2 and mDia physically interact and cross-regulate in cultured cells (Sun et al., 2013, 2011), we propose that the conserved EXC-5–CDC-42 pathway modulates their physical interaction and that this regulation and interaction are functionally important *in vivo* during tubulogenesis.

Model for how the EXC-5–CDC-42 pathway regulates a formin network during EC tubulogenesis

Our data suggest a model for regulatory interactions within this pathway that has six components labeled in Fig. 5A. (1) EXC-5, the ortholog of FGD, functions via the Rho GTPase CDC-42 to promote outgrowth in parallel with EXC-6/INF2. (2) The formins CYK-1/mDia and INFT-2/INF2 are regulated by the EXC-5–CDC-42 pathway and in turn regulate EC outgrowth. (3) CYK-1 inhibits INFT-2, probably by regulating INFT-2 accumulation, which (4) modulates the actin-polymerizing function of INFT-2. (5) CYK-1 and INFT-2 also act as redundant negative regulators of basolateral outgrowth, as canals overgrow in *cyk-1(ts); inft-2(0)* mutants. (6) Because CDC-42 has been suggested to modulate endocytic trafficking (Lant et al., 2015; Mattingly and Buechner, 2011), we speculate that the CDC-42-promoted Venus::CYK-1 punctae are endocytic vesicles, and that accumulation of F-actin in these punctae might reflect another mechanism by which CYK-1 regulates F-actin levels.

One possible mechanism for modulating F-actin levels upon loss of CYK-1 or INFT2 is suggested by studies in fission yeast, where loss of one actin-polymerizing factor may promote the activity of another indirectly by increasing the pool of available cytoplasmic actin (Burke et al., 2014). However, in yeast this mechanism seems non-specific, as loss of one actin-polymerizing factor leads to increased activity of several others (Burke et al., 2014). By contrast, our observations in the EC suggests that there is specificity, as loss of INFT-2, unlike reduction of CYK-1, does not lead to increased F-actin accumulation.

We therefore favor an alternative model in which the CYK-1-mediated inhibition of INFT-2 is specific and direct (Fig. 5B). This model is based on the fact that *in vitro* and in cell culture, binding of the INF2-DID to the mDia-DAD inhibits mDia actin-polymerizing activity (Sun et al., 2013, 2011). We note that in the partial INFT-2-DID, the residues important for INF2-DID binding to the mDia-DAD, which are mutated in patients with autosomal dominant

Development (2016) 143, 4173-4181 doi:10.1242/dev.141861

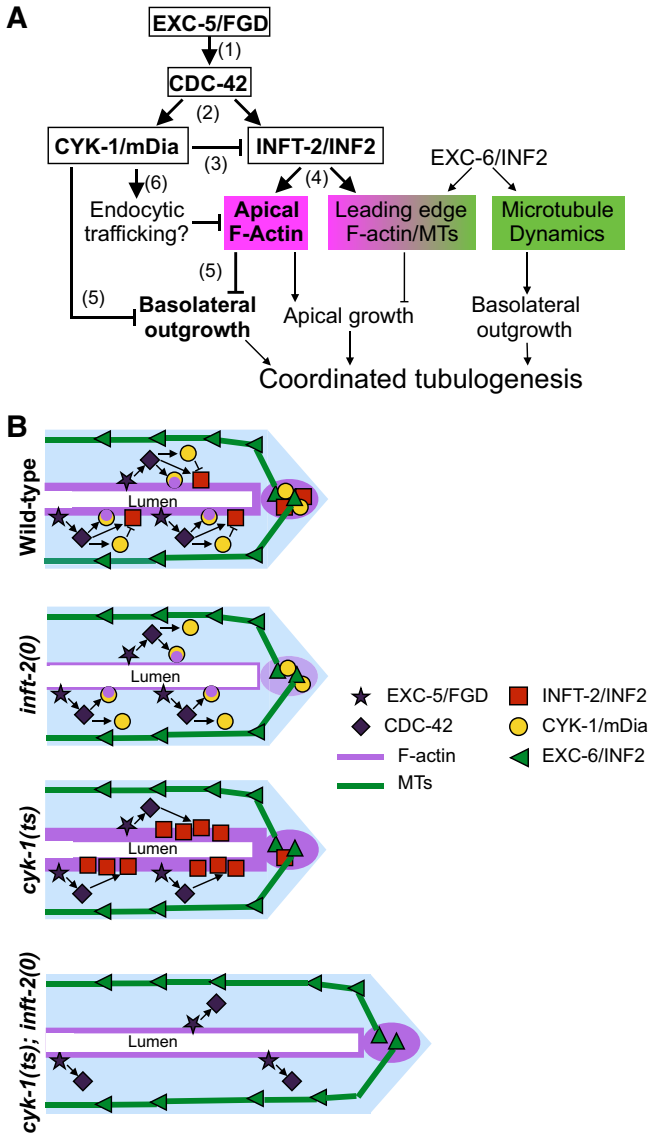

Fig. 5. An *exc-5-cdc-42*-regulated formin network modulates tubulogenesis in the EC. (A,B) Genetic (A) and cellular (B) models for the role and regulation of INF2 and diaphanous formins in EC tubulogenesis. (A) We propose that CYK-1/mDia and INFT-2/INF2 regulate F-actin-based structures (magenta), whereas EXC-6/INF2 regulates microtubule (MT)-based structures (green) (see also Shaye and Greenwald, 2015). (B) At the cellular level, we previously showed that EXC-6/INF2 (green triangles) accumulates at the leading edge and along basolateral microtubules, regulating microtubule dynamics and promoting EC outgrowth (Shaye and Greenwald, 2015). Here we have shown that EXC-5/FGD (purple stars) and CDC-42 (diamonds) regulate CYK-1/mDia (yellow circles) and INFT-2/INF2 (red squares). CYK-1/mDia is found in the cytoplasm and at the leading edge, and can form punctae, some of which accumulate F-actin. INFT-2/INF2 is found along the apical F-actin cytoskeleton, as well as colocalizing with F-actin at the leading edge. We note that there may be other EXC-5/FGD-CDC-42 targets, because the *exc-5(0)* outgrowth and cystic phenotypes were not seen in *inft-2(0)* or *cyk-1(ts)* single or double mutants. In *inft-2(0)* mutants, F-actin levels are significantly reduced, whereas in *cyk-1(ts)* mutants F-actin levels are greatly increased, dependent on *inft-2* activity. We therefore propose that CYK-1 and INFT-2 modulate outgrowth at least in part by fine-tuning the levels of apical and leading-edge F-actin. When this regulatory mechanism is lost, as in *cyk-1(ts); inft-2(0)* double mutants, the outgrowth-promoting activities of EXC-6/INF2, and perhaps other EXC-5-CDC-42 target(s), are not properly regulated, resulting in excessive outgrowth.

FSGS, are conserved (Fig. S2). Therefore, direct binding between the INFT-2-DID and the CYK-1-DAD might also occur. Importantly, in the EC we found that CYK-1 inhibits the actin-polymerizing activity of INFT-2; the reciprocal effect to that seen in previous studies (Sun et al., 2013, 2011). Whether this reciprocal effect can also be observed with human mDia and INF2 will require more precise *in vitro* and cell culture studies.

It has recently been shown that mDia acts upstream of INF2 to promote its microtubule-stabilizing activity, and direct binding of the INF2-DID to the mDia-DAD for this function was suggested by the requirement for INF2-DID residues important for mDia-DAD-binding (Bartolini et al., 2016). It is known that INF2 can bind to microtubules and F-actin simultaneously *in vitro* (Gaillard et al., 2011), raising the question of how these two INF2 activities (microtubule stabilization and F-actin polymerization) are regulated and coordinated. Based on our results, and those of Bartolini et al. (2016), it is tempting to speculate that mDia acts as a 'switch' to modulate INF2 function, such that mDia binding to INF2 inhibits its actin-polymerizing function, perhaps by regulating INF2 accumulation as we have seen in the EC, and concomitantly promotes other functions, such as microtubule stabilization.

Potential implications for human disease

Like EXC-5 in EC tubulogenesis, members of the mammalian FGD family have been implicated in various tubulogenic processes, such as vascular development (Cheng et al., 2012; Daubon et al., 2011; Kurogane et al., 2012). Moreover, recessive loss-of-function mutations in *FGD4* underlie a CMT neuropathy that exhibits cellular phenotypes similar to those caused by dominant gain-of-function mutations in *INF2* (De Sandre-Giovannoli et al., 2005; Delague et al., 2007; Fabrizi et al., 2009; Mathis et al., 2014). Our model suggests a parsimonious explanation for how recessive mutations in *FGD4* and dominant mutations in *INF2* might cause similar phenotypes.

Previously, it was proposed that the interaction between INF2 and mDia inhibits the actin-polymerizing activity of mDia, and that disruption of this interaction, triggered by disease-causing mutations in the INF2-DID, resulted in excessive mDia activity and disease (Sun et al., 2014, 2013, 2011). However, in this model, it is difficult to envision how mutations that disrupt the ability of INF2 to bind to, and inhibit, mDia would result in a dominant phenotype, as the remaining wild-type *INF2* copy in heterozygous patients should be able to provide mDia-inhibiting activity. Instead, our model in which mDia is a target of FGD/Cdc42 signaling that inhibits the actin-polymerizing activity of INF2 provides a straightforward explanation for the genetic properties of disease-causing mutations: recessive, loss-of-function mutations in *FGD4* may lead to decreased activation of mDia and hence promote INF2 actin-polymerizing function. Similarly, gain-of-function mutations in *INF2*, which disrupt the INF2-mDia interaction (Sun et al., 2011), would lead to loss of mDia-mediated INF2 inhibition in a dominant manner. In both cases, the effect of the mutations would be predicted to cause excessive F-actin accumulation, a hallmark of *INF2*-associated dominant CMT neuropathy (Mathis et al., 2014), and perhaps to defects in microtubule dynamics (Bartolini et al., 2016), which we have proposed might also contribute to *INF2*-associated diseases (Shaye and Greenwald, 2015).

MATERIALS AND METHODS

Strains and transgenes

Full genotypes are listed in Table S1. Alleles and balancer chromosomes are described in WormBase (http://www.wormbase.org/). Primers used to

Development (2016) 143, 4173-4181 doi:10.1242/dev.141861

confirm genotypes are listed in Table S3. The following alleles, balancers and transgenic markers were used:

LGII: *cdc-42(gk388)* (a 478 bp deletion that removes part of the 5′ upstream region and the first exon, thus deleting transcription and translation start sites), *mIn1[mIs14]*

LGIII: *exc-6(gk386)* (a 1345 bp deletion that removes part of the 5′ upstream region, the entire first and part of the second exon), *cyk-1 (ok2300)* (an 827 bp deletion that removes the FH2 domain, and sequences C-terminal to this domain), *cyk-1(or596ts)*, *qC1[nIs189]*

LGIV: *exc-5(rh232)* [a 4564 bp deletion that removes the first 12-13, out of 16-17, exons (depending on the isoform)], *nT1[qIs51]*

LGV: *inft-2(ok1296)* (a 719 bp deletion that removes the FH1 and FH2 domains, and sequences C-terminal to these domains), *nT1[qIs51]*

LGX: *arIs198* (Shaye and Greenwald, 2015)

Unmapped: *arIs195* (Shaye and Greenwald, 2015).

All transgenes generated in this study, and the plasmids used derive them, are described in Table S2. See supplementary Materials and Methods for further details.

Molecular biology

Standard methods were used for PCR and cloning. Table S3 lists all primers used for cloning and sequencing the constructs generated. We amplified the cDNAs for *exc-5* and *inft-1* from the ProQuest *C. elegans* cDNA library (Life Technologies) and the cDNA for *cyk-1* was kindly provided by D. Pruyne (SUNY Upstate Medical University, NY, USA).

Phenotypic analysis

Analysis of all strains in Fig. 1 was performed with animals grown at 25°C and scored by wide-field microscopy. For transgenes visualized in Fig. 2B, C,D,F, animals were grown at 22 or 25°C and imaged by spinning disk confocal microscopy (see below). All strains in Figs 3 and 4 were analyzed using a temperature-shift strategy: adult hermaphrodites were allowed to lay eggs at 15°C for ∼24 h, then the adults were removed and F1 embryos were grown at 25°C, the restrictive temperature (Davies et al., 2014; Jordan et al., 2016), until L4 to young adult stage, when they were scored. We always examined the youngest animals in our temperature-shift experiments (i.e. L4s or young adults, from plates that contained many gravid adults), in order to score only those animals that had been subjected to the non-permissive temperature since the earliest stages of embryogenesis. Strains in Fig. 3 were scored by wide-field microscopy, and those in Fig. 4 were scored by spinning disk confocal microscopy.

Wide-field microscopy

Larvae were mounted on 5% agarose pads using 12.5 µM levamisole in M9 buffer as anesthetic. Phenotypes were scored using a Zeiss Axio Imager Z1 microscope through a Plan-Apochromat 40×/1.4 oil objective. Photomicrographs in Fig. 1 were taken through an EC Plan-Neofluar 10×/0.3 NA objective using a Hamamatsu ORCA-ER camera. Fluorescence illumination was provided by an X-Cite 120Q light source (EXFO Photonic Solutions). Images were processed with Fiji/ImageJ (http://imagej.nih.gov/ij/index.html).

Spinning disk confocal microscopy

Larvae were mounted as described above for wide-field microscopy, imaged using a Yokagawa CSU-10 spinning disk unit mounted on a Zeiss Cell Observer Z1, and filmed with a Photometrics Evolve EMCCD camera. Photomicrographs in Fig. 2 and Fig. 4C, and those used to make Movies 1-3, were taken using a Plan-Apochromat 63×/1.4 oil objective. Photomicrographs in Fig. 3 and Fig. 4A were taken using a Plan-Apochromat 40×/1.4 oil objective. Acquisition settings for each transgene are listed below or in the supplementary Materials and Methods. Images were processed with Fiji/ImageJ.

Quantification of Venus::INFT-2 accumulation

Wild type and mutants carrying *arEx2406* were grown and imaged as described in supplementary Materials and Methods. Between four and ten 1 µm *z*-sections were taken for each sample, and maximum projections were generated in Fiji/ImageJ to ensure capturing the entire width of the EC canal being measured. Because Venus::INFT-2 was expressed from an extrachromosomal array, Venus levels between animals were variable and images were processed to enhance contrast/brightness. We note that this processing was linear and applied to the entire field of each sample, so the same processing occurred at the apical and cytoplasmic regions and should not affect measurements. In Fiji/ImageJ we selected an 'apical' region-of-interest (ROI), as the region overlapping LifeAct::TagRFP, and a similarly sized 'cytoplasmic' ROI outside the region marked with LifeAct::TagRFP. We measured Venus fluorescence in the two regions and calculated the ratio of apical to cytoplasmic fluorescence. This measurement is internally controlled, as differences in expression levels from animal to animal should not affect the ratio of apical versus cytoplasmic levels in a given individual.

Quantification of LifeAct::TagRFP levels

Wild type and mutants carrying *arIs198* were grown in parallel and subjected to temperature shift as described above. Larvae were mounted and filmed by live spinning disk confocal microscopy as described above. Acquisition settings for all genotypes were: CFP (445 nm) laser power at 3.3%, EM gain 600, and exposure 100 ms; TagRFP (561 nm) laser power at 10.8%, EM gain 570, exposure 300 ms. Representative pictures shown in Fig. 4A are maximum projections of five to eight 0.5 µm *z*-steps. Images used for quantification were not projected or processed. We used Fiji/ImageJ to select an ROI that encompassed the 'tip' and 'canal' regions, and measured fluorescence intensity within the ROI for CFP and TagRFP channels as described in the legend for Fig. 4B.

Acknowledgements

We thank David Pruyne for the *cyk-1* cDNA; Julie Canman for the *cyk-1(ts)* allele; Michelle Attner, Julie Canman and Claire de la Cova for comments; Daniel Raps and Xinlan Zhou for technical help; and Jan Kitajewski for support and encouragement. Some strains were provided by the CGC, which is funded by the NIH Office of Research Infrastructure Programs (P40 OD010440).

Competing interests

The authors declare no competing or financial interests.

Author contributions

D.D.S. and I.G. conceived and designed the experiments, analyzed the data, and wrote the manuscript. D.D.S. performed the experiments.

Funding

This work was funded by the Howard Hughes Medical Institute, for which D.D.S was a Research Specialist and I.G. an Investigator; and a Senior Scholar Award from the Ellison Medical Foundation [AG-SS-2951-12 to I.G.]. Deposited in PMC for release after 6 months.

Supplementary information

Supplementary information available online at
http://dev.biologists.org/lookup/doi/10.1242/dev.141861.supplemental

References

Bartolini, F., Andres-Delgado, L., Qu, X., Nik, S., Ramalingam, N., Kremer, L., Alonso, M. A. and Gundersen, G. G. (2016). An mDia1-INF2 formin activation cascade facilitated by IQGAP1 regulates stable microtubules in migrating cells. *Mol. Biol. Cell* **27**, 1797-1808.

Boyer, O., Nevo, F., Plaisier, E., Funalot, B., Gribouval, O., Benoit, G., Cong, E. H., Arrondel, C., Tête, M.-J., Montjean, R. et al. (2011). INF2 mutations in Charcot–Marie–Tooth disease with glomerulopathy. *N. Engl. J. Med.* **365**, 2377-2388.

Breitsprecher, D. and Goode, B. L. (2013). Formins at a glance. *J. Cell Sci.* **126**, 1-7.

Brown, E. J., Schlöndorff, J. S., Becker, D. J., Tsukaguchi, H., Uscinski, A. L., Higgs, H. N., Henderson, J. M. and Pollak, M. R. (2010). Mutations in the formin gene INF2 cause focal segmental glomerulosclerosis. *Nat. Genet.* **42**, 72-76.

Buechner, M., Hall, D. H., Bhatt, H. and Hedgecock, E. M. (1999). Cystic canal mutants in *Caenorhabditis elegans* are defective in the apical membrane domain of the renal (excretory) cell. *Dev. Biol.* **214**, 227-241.

Burke, T. A., Christensen, J. R., Barone, E., Suarez, C., Sirotkin, V. and Kovar, D. R. (2014). Homeostatic actin cytoskeleton networks are regulated by assembly factor competition for monomers. *Curr. Biol.* **24**, 579-585.

Chalkia, D., Nikolaidis, N., Makalowski, W., Klein, J. and Nei, M. (2008). Origins and evolution of the formin multigene family that is involved in the formation of actin filaments. *Mol. Biol. Evol.* **25**, 2717-2733.

Cheng, C., Haasdijk, R., Tempel, D., van de Kamp, E. H. M., Herpers, R., Bos, F., Den Dekker, W. K., Blonden, L. A. J., de Jong, R., Burgisser, P. E. et al. (2012). Endothelial cell-specific FGD5 involvement in vascular pruning defines neovessel fate in mice. *Circulation* **125**, 3142-3158.

Courtemanche, N., Pollard, T. D. and Chen, Q. (2016). Avoiding artefacts when counting polymerized actin in live cells with LifeAct fused to fluorescent proteins. *Nat. Cell Biol.* **18**, 676-683.

Daubon, T., Buccione, R. and Génot, E. (2011). The Aarskog-Scott syndrome protein Fgd1 regulates podosome formation and extracellular matrix remodeling in transforming growth factor β-stimulated aortic endothelial cells. *Mol. Cell. Biol.* **31**, 4430-4441.

Davies, T., Jordan, S. N., Chand, V., Sees, J. A., Laband, K., Carvalho, A. X., Shirasu-Hiza, M., Kovar, D. R., Dumont, J. and Canman, J. C. (2014). High-resolution temporal analysis reveals a functional timeline for the molecular regulation of cytokinesis. *Dev. Cell* **30**, 209-223.

De Sandre-Giovannoli, A., Delague, V., Hamadouche, T., Chaouch, M., Krahn, M., Boccaccio, I., Maisonobe, T., Chouery, E., Jabbour, R., Atweh, S. et al. (2005). Homozygosity mapping of autosomal recessive demyelinating Charcot-Marie-Tooth neuropathy (CMT4H) to a novel locus on chromosome 12p11.21-q13.11. *J. Med. Genet.* **42**, 260-265.

Delague, V., Jacquier, A., Hamadouche, T., Poitelon, Y., Baudot, C., Boccaccio, I., Chouery, E., Chaouch, M., Kassouri, N., Jabbour, R. et al. (2007). Mutations in FGD4 encoding the Rho GDP/GTP exchange factor FRABIN cause autosomal recessive Charcot-Marie-Tooth type 4H. *Am. J. Hum. Genet.* **81**, 1-16.

Fabrizi, G. M., Taioli, F., Cavallaro, T., Ferrari, S., Bertolasi, L., Casarotto, M., Rizzuto, N., Deconinck, T., Timmerman, V. and De Jonghe, P. (2009). Further evidence that mutations in FGD4/frabin cause Charcot-Marie-Tooth disease type 4H. *Neurology* **72**, 1160-1164.

Gaillard, J., Ramabhadran, V., Neumanne, E., Gurel, P., Blanchoin, L., Vantard, M. and Higgs, H. N. (2011). Differential interactions of the formins INF2, mDia1, and mDia2 with microtubules. *Mol. Biol. Cell* **22**, 4575-4587.

Gao, J., Estrada, L., Cho, S., Ellis, R. E. and Gorski, J. L. (2001). The *Caenorhabditis elegans* homolog of FGD1, the human Cdc42 GEF gene responsible for faciogenital dysplasia, is critical for excretory cell morphogenesis. *Hum. Mol. Genet.* **10**, 3049-3062.

Hayakawa, M., Matsushima, M., Hagiwara, H., Oshima, T., Fujino, T., Ando, K., Kikugawa, K., Tanaka, H., Miyazawa, K. and Kitagawa, M. (2008). Novel insights into FGD3, a putative GEF for Cdc42, that undergoes SCF(FWD1/beta-TrCP)-mediated proteasomal degradation analogous to that of its homologue FGD1 but regulates cell morphology and motility differently from FGD1. *Genes Cells* **13**, 329-342.

Huber, C., Martensson, A., Bokoch, G. M., Nemazee, D. and Gavin, A. L. (2008). FGD2, a CDC42-specific exchange factor expressed by antigen-presenting cells, localizes to early endosomes and active membrane ruffles. *J. Biol. Chem.* **283**, 34002-34012.

Iruela-Arispe, M. L. and Beitel, G. J. (2013). Tubulogenesis. *Development* **140**, 2851-2855.

Jordan, S. N., Davies, T., Zhuravlev, Y., Dumont, J., Shirasu-Hiza, M. and Canman, J. C. (2016). Cortical PAR polarity proteins promote robust cytokinesis during asymmetric cell division. *J. Cell Biol.* **212**, 39-49.

Kühn, S. and Geyer, M. (2014). Formins as effector proteins of Rho GTPases. *Small GTPases* **5**, e29513.

Kurogane, Y., Miyata, M., Kubo, Y., Nagamatsu, Y., Kundu, R. K., Uemura, A., Ishida, T., Quertermous, T., Hirata, K. and Rikitake, Y. (2012). FGD5 mediates proangiogenic action of vascular endothelial growth factor in human vascular endothelial cells. *Arterioscler. Thromb. Vasc. Biol.* **32**, 988-996.

Lant, B., Yu, B., Goudreault, M., Holmyard, D., Knight, J. D. R., Xu, P., Zhao, L., Chin, K., Wallace, E., Zhen, M. et al. (2015). CCM-3/STRIPAK promotes seamless tube extension through endocytic recycling. *Nat. Commun.* **6**, 6449.

Liu, R., Linardopoulou, E. V., Osborn, G. E. and Parkhurst, S. M. (2010). Formins in development: orchestrating body plan origami. *Biochim. Biophys. Acta* **1803**, 207-225.

Madrid, R., Aranda, J. F., Rodríguez-Fraticelli, A. E., Ventimiglia, L., Andrés-Delgado, L., Shehata, M., Fanayan, S., Shahheydari, H., Gómez, S., Jiménez, A. et al. (2010). The formin INF2 regulates basolateral-to-apical transcytosis and lumen formation in association with Cdc42 and MAL2. *Dev. Cell* **18**, 814-827.

Mathis, S., Funalot, B., Boyer, O., Lacroix, C., Marcorelles, P., Magy, L., Richard, L., Antignac, C. and Vallat, J.-M. (2014). Neuropathologic characterization of INF2-related Charcot-Marie-tooth disease: evidence for a schwann cell actinopathy. *J. Neuropathol. Exp. Neurol.* **73**, 223-233.

Mattingly, B. C. and Buechner, M. (2011). The FGD homologue EXC-5 regulates apical trafficking in *C.* elegans tubules. *Dev. Biol.* **359**, 59-72.

Mi-Mi, L., Votra, S., Kemphues, K., Bretscher, A. and Pruyne, D. (2012). Z-line formins promote contractile lattice growth and maintenance in striated muscles of *C. elegans*. *J. Cell Biol.* **198**, 87-102.

Miyamoto, Y., Yamauchi, J. and Itoh, H. (2003). Src kinase regulates the activation of a novel FGD-1-related Cdc42 guanine nucleotide exchange factor in the signaling pathway from the endothelin A receptor to JNK. *J. Biol. Chem.* **278**, 29890-29900.

Riedl, J., Crevenna, A. H., Kessenbrock, K., Yu, J. H., Neukirchen, D., Bista, M., Bradke, F., Jenne, D., Holak, T. A., Werb, Z. et al. (2008). Lifeact: a versatile marker to visualize F-actin. *Nat. Methods* **5**, 605-607.

Sarov, M., Murray, J. I., Schanze, K., Pozniakovski, A., Niu, W., Angermann, K., Hasse, S., Rupprecht, M., Vinis, E., Tinney, M. et al. (2012). A genome-scale resource for in vivo tag-based protein function exploration in *C. elegans*. *Cell* **150**, 855-866.

Shaye, D. D. and Greenwald, I. (2015). The disease-associated formin INF2/EXC-6 organizes lumen and cell outgrowth during tubulogenesis by regulating F-actin and microtubule cytoskeletons. *Dev. Cell* **32**, 743-755.

Steenblock, C., Heckel, T., Czupalla, C., Espirito Santo, A. I., Niehage, C., Sztacho, M. and Hoflack, B. (2014). The Cdc42 guanine nucleotide exchange factor FGD6 coordinates cell polarity and endosomal membrane recycling in osteoclasts. *J. Biol. Chem.* **289**, 18347-18359.

Sun, H., Schlondorff, J. S., Brown, E. J., Higgs, H. N. and Pollak, M. R. (2011). Rho activation of mDia formins is modulated by an interaction with inverted formin 2 (INF2). *Proc. Natl. Acad. Sci. USA* **108**, 2933-2938.

Sun, H., Schlondorff, J., Higgs, H. N. and Pollak, M. R. (2013). Inverted formin 2 regulates actin dynamics by antagonizing Rho/diaphanous-related formin signaling. *J. Am. Soc. Nephrol.* **24**, 917-929.

Sun, H., Al-Romaih, K. I., MacRae, C. A. and Pollak, M. R. (2014). Human kidney disease-causing INF2 mutations perturb Rho/Dia signaling in the glomerulus. *EBioMedicine* **1**, 107-115.

Sundaram, M. V. and Buechner, M. (2016). The *Caenorhabditis elegans* excretory system: a model for tubulogenesis, cell fate specification, and plasticity. *Genetics* **203**, 35-63.

Sundaram, M. V. and Cohen, J. D. (2016). Time to make the doughnuts: Building and shaping seamless tubes. *Semin. Cell Dev. Biol.* S1084-9521(16)30130-6.

Suzuki, N., Buechner, M., Nishiwaki, K., Hall, D. H., Nakanishi, H., Takai, Y., Hisamoto, N. and Matsumoto, K. (2001). A putative GDP-GTP exchange factor is required for development of the excretory cell in *Caenorhabditis elegans*. *EMBO Rep.* **2**, 530-535.

Umikawa, M., Obaishi, H., Nakanishi, H., Satoh-Horikawa, K., Takahashi, K., Hotta, I., Matsuura, Y. and Takai, Y. (1999). Association of frabin with the actin cytoskeleton is essential for microspike formation through activation of Cdc42 small G protein. *J. Biol. Chem.* **274**, 25197-25200.

Young, K. G., Thurston, S. F., Copeland, S., Smallwood, C. and Copeland, J. W. (2008). INF1 is a novel microtubule-associated formin. *Mol. Biol. Cell* **19**, 5168-5180.

Zheng, Y., Fischer, D. J., Santos, M. F., Tigyi, G., Pasteris, N. G., Gorski, J. L. and Xu, Y. (1996). The faciogenital dysplasia gene product FGD1 functions as a Cdc42Hs-specific guanine-nucleotide exchange factor. *J. Biol. Chem.* **271**, 33169-33172.

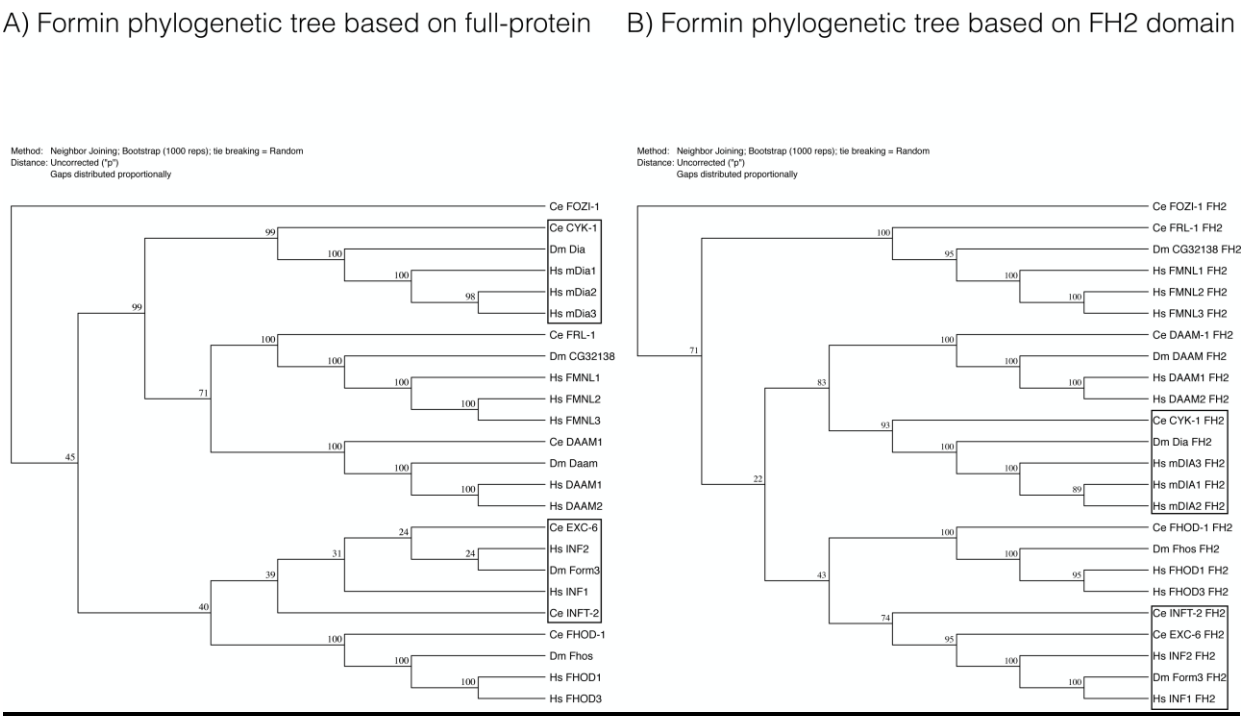

Fig. S1. Phylogenetic analyses of *C. elegans* (Ce), *Drosophila* (Dm) and human (Hs) formins. We generated phylogenetic trees using **(A)** the full-length sequences or **(B)** the FH2 domain alone, as had been previously done (Chalkia et al., 2008; Liu et al., 2010; Mi-Mi et al., 2012). In both panels, the mDia and INF2 families are highlighted. Protein sequences were aligned using the ClustalW function of MacVector (MacVector, Inc. Apex, NC. USA), using the Gonnet matrix with default settings. Phylogenetic trees were generated in MacVector using the neighbor joining method with 1000 bootstrap repetitions. Percent branch support is shown for all branches. We rooted the trees with Ce FOZI-1, a highly divergent formin-like nuclear protein that influences cell fate choices but does not interact with actin (Johnston et al., 2006). We note that for the INF2 family, using full-length sequences provides low bootstrap support for branching, likely due to divergence in sequences outside the catalytic FH1/FH2 domains. However, both *C. elegans* INF2 paralogs clearly cluster within this family, and using the FH2 domain alone to elucidate relationships between INF2 family members provides more reliable clustering.

Mutated in FSGS (Brown, et al., 2010; Boyer et al., 2011a). Shaded (E184 and R218) are required in INF2-DID for interaction with mDia-DAD (Sun, et. al., 2011).

Mutated in FSGS + CMT (Boyer, et al., 2011b).

Mediate intramolecular DID-DAD interaction in mouse mDia1 (Nezami, et al., 2006).

Fig. S2. Residues required for intra- and inter-molecular DID/DAD interactions, and residues mutated in human disease, are conserved in the divergent INFT-2 "DID". Alignment of the DID regions of human (Hs) INF2 and *C. elegans* (Ce) INFT-2. We used the mouse (Mm) mDia1 DID sequence as a reference, because it has been crystallized bound to its DAD and used to define DID/DAD interacting residues (Nezami et al., 2006). These residues are highlighted in blue here. We note that many of these are conserved in the divergent INFT-2 DID, including some that when mutated affect mDia DID/DAD interactions (e.g. mDia1 Ile222, corresponding to INFT-2 Ile214, mDia1 Ile259, corresponding to INFT-2 Val258, and mDia1 Leu260, corresponding to INFT-2 Leu 259). Residues mutated in INF2 that lead to FSGS or FSGS+CMT are highlighted in Green and Red, respectively. The two residues tested that affected INF2-DID to mDia-DAD interaction (Sun et al., 2011), Glu184 and Arg218, are conserved in Ce INFT-2 (shaded).

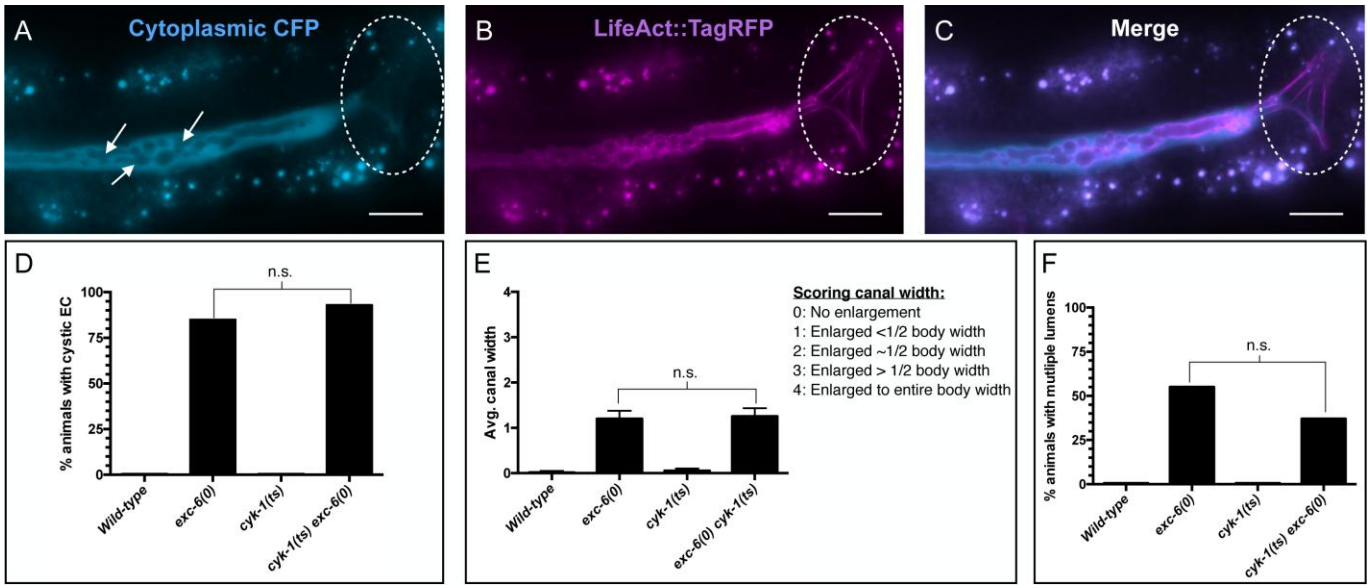

Fig. S3. Phenotypes in *cyk-1(ts) exc-6(0)* double mutants resemble those seen in *exc-6(0)* alone. Photomicrographs **(A-C)** showing multiple lumens (arrows) and a disorganized F-actin structure at the leading edge (dashed circle), both characteristic phenotypes of *exc-6(0)* mutants (Shaye and Greenwald, 2015). Images were acquired via wide-field microscopy, using a Plan-Apochromat 40x/1.4 Oil objective, as described in Materials and Methods. Scale bar is 10µm. Quantification of the **(E)** penetrance and **(F)** severity of the cystic phenotype, as well as the **(G)** penetrance of the multiple lumen phenotype in *wild-type* (n=30), *exc-6(0)* (n=60), *cyk-1(ts)* (n=60) and *cyk-1(ts) exc-6(0)* doubles (n=43). Significance for penetrance of cystic and multiple lumen phenotypes was calculated by a two-tailed Fisher's exact test. Significance for the severity of the cystic phenotype was calculated with a Mann-Whitney test.

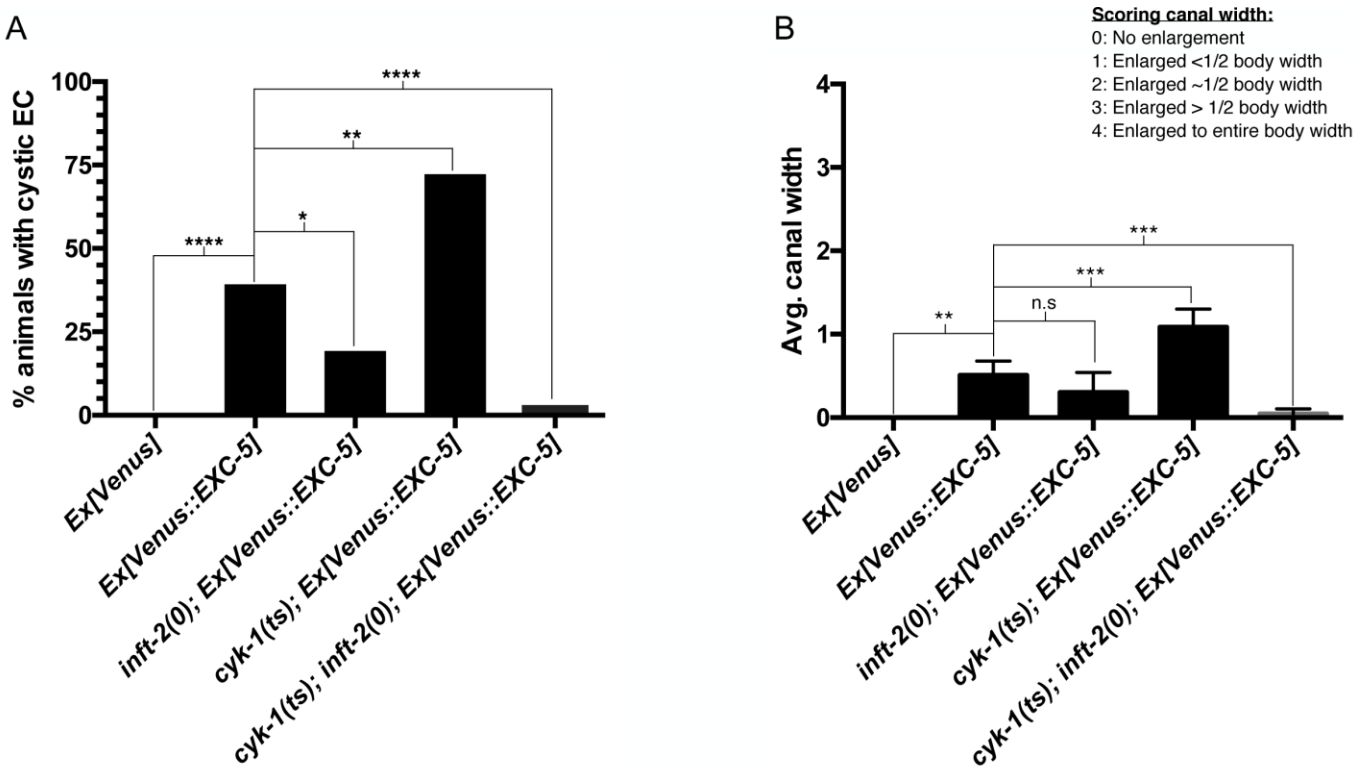

Fig. S4. Other phenotypes caused by Venus::EXC-5 overexpression are also modified by *inft-2(0)* and *cyk-1(ts)*. Quantification of the **(A)** penetrance and **(B)** severity of the cystic phenotype in *wild-type* carrying *arEx2404* (*Ex[Venus]* n=30), *wild-type* carrying *arEx2360* (*Ex[Venus::EXC-5]* n=65), *inft-2(0); arEx2360* (n=30), *cyk-1(ts); arEx2360* (n=60) and *cyk-1(ts); inft-2(0); arEx2360* (n=46). Significance for penetrance the cystic phenotype was calculated by a two-tailed Fisher's exact test. Significance for the severity of the cystic phenotype was calculated with a Kruskal-Wallis test for multiple comparisons.

Movie 1. Venus::CYK-1 (yellow) is cytoplasmic and is also found in dynamic juxta-apical punctae in *wild-type*. Arrows mark the first appearance of punctae that were visible for at least two frames (~90 seconds). In this ~10-minute movie we counted at least 12 such punctae. F-actin, labelled with LifeAct::TagRFP (magenta), is found at the lumen-lining apical membrane, and can be seen accumulating in some of the juxta-apical Venus::CYK-1 labelled punctae. This movie is a maximum projection of seventeen 1µm z-steps taken using the settings for Venus::CYK-1 described in the "Spinning Disk Microscopy Settings" section of the Supplementary Materials and Methods.

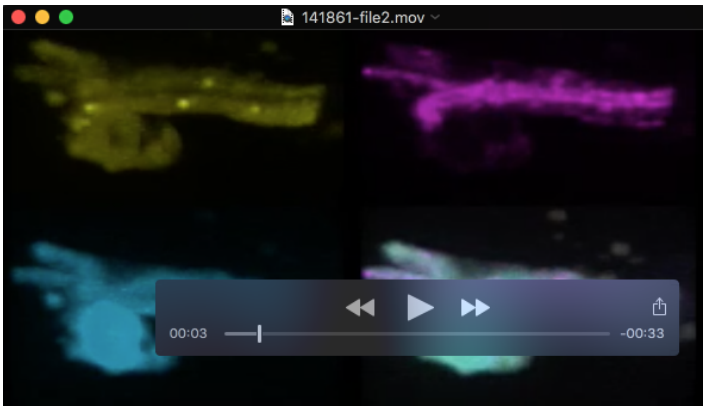

Movie 2. 3D projection of the same *wild-type* EC seen in Fig. 2F, showing that that when not present in juxta-apical punctae, Venus::CYK-1 appears cytoplasmic and reaches the basolateral side (entire cytoplasm is marked by CFP). Eight 1.0µm thick sections were used to generate this projection, and images were acquired as described for Venus::CYK-1 in the "Spinning Disk Microscopy Settings" section of the Supplementary Materials and Methods.

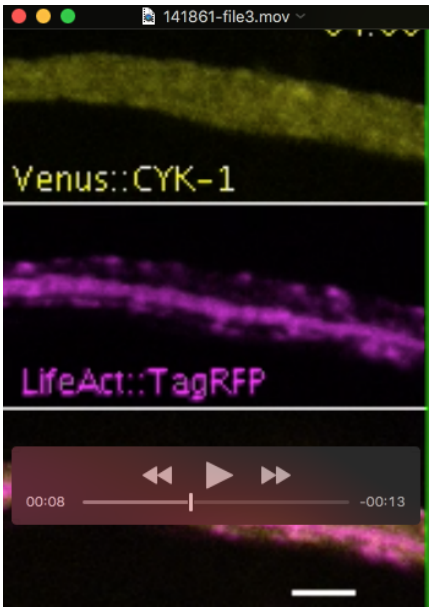

Movie 3. Venus::CYK-1 (yellow) accumulation in juxta-apical punctae is greatly reduced in *cdc-42(0*)*. Arrows mark the first appearance of punctae that were visible for at least two frames (~60 seconds). In this ~10-minute movie we only found 2 such punctae, and both were found near the basolateral domain, not juxta-apical (compare to *wild-type* Movie S1). F-actin, labelled with LifeAct::TagRFP (magenta), is found at the lumen-lining apical membrane and can be seen accumulating in some motile punctae, although most are not marked with Venus::CYK-1 and their localization is more variable than in *wild-type*. This movie is a maximum projection of four 1µm z-steps taken using the settings for Venus::CYK-1 described in the "Spinning Disk Microscopy Settings" section of the Supplementary Materials and Methods.

Supplementary Materials and Methods

Strains

Standard methods were used for strain handling and maintenance (Brenner, 1974). Mutant alleles are described in WormBase (www.wormbase.org). Primers used to confirm genotypes by sequencing or PCR are listed in the "Primers" table below. The following GFP-marked balancer chromosomes were used in crosses and to maintain sterile or lethal mutants: *mIn1[mIs14]*, *hT2[qIs48]*, *nT1[qIs51]* (Edgley et al., 2006), and *qC1[nIs189]* (Andersen et al., 2008).

Table S1. Strains

Strain	Genotype*	Figure(s)
GS6602	*arIs198*	1A, G. 3A, B. 4A, B
GS7284	*exc-6(gk386); arIs198*	1B, G. 3A
GS7022	*exc-5(rh232); arIs198*	1C, G. 4A, B
GS7266	*exc-6(gk386); exc-5(rh232); arIs198*	1D, G
GS8109	*cdc-42(gk388)/mIn1[mIs14]; arIs198*	1E, G
GS8110	*cdc-42(gk388)/mIn1[mIs14]; exc-6(gk386); arIs198*	1F, G
GS8124	*arIs195; arEx2360*	1H, J
GS8125	*cdc-42(gk388)/mIn1[mIs14]; arIs195; arEx2360*	1I, J
GS8122	*arIs195; arEx2411*	1J
GS7924	*arIs195; arEx2348*	2B
GS8115	*arIs198; arEx2406*	2C
GS8126	*cdc-42(gk388)/mIn1[mIs14]*; *arIs198; arEx2406*	2C
GS7933	*arIs195; arEx2357*	2D
GS8119	*arIs198; arEx2410*	2E
GS8127	*cdc-42(gk388)/mIn1[mIs14]*; *arIs198; arEx2410*	2E
GS6716	*inft-2(ok1296); arIs198*	3A. 4A, B
GS7637	*cyk-1(or596ts); arIs198*	3A. 4A, B
GS7025	*exc-6(gk386); inft-2(ok1296); arIs198*	3A
GS7638	*cyk-1(or596ts) exc-6(gk386); arIs198*	3A
GS7959	*cyk-1(or596ts); inft-2(ok1296); arIs198*	3A, C. 4A, B
GS7960	*cyk-1(or596ts) exc-6(gk386); inft-2(ok1296); arIs198*	3A
GS8113	*arIs198; arEx2404*	3D, 3E
GS8150	*cyk-1(or596ts); inft-2(ok1296); arIs198; arEx2404*	3D
GS8151	*cyk-1(or596ts); inft-2(ok1296); arIs198; arEx2406*	3D, 4C, D
GS8152	*cyk-1(or596ts); inft-2(ok1296); arIs198; arEx2410*	3D
GS7953	*arIs198; arEx2360*	3E
GS8120	*inft-2(ok1296); arIs198; arEx2360*	3E
GS8146	*cyk-1(or596ts); arIs198; arEx2360*	3E
GS8147	*cyk-1(or596ts); inft-2(ok1296); arIs198; arEx2360*	3E
GS8105	*cyk-1(ok2300)/qC1[nIs189]; arIs198*	Not shown
GS8106	*exc-6(gk386) cyk-1(ok2300)/exc-6(gk386) qC1[nIs189]; arIs198*	Not shown
GS8107	*cyk-1(ok2300)/qC1[nIs189]; inft-2(ok1296); arIs198*	Not shown

***:** Integrated *arIs* transgenes rescue *unc-119(ed3)*, and extrachromosomal *arEx* transgenes rescue *pha-1(e2123ts)*. These mutations may be present in some backgrounds for transgene selection. Full genotypes available on request.

Transgenes and Plasmids

Details of plasmid constructions are available upon request. Extrachromosomal transgenes were generated by germline micro-injection of plasmid mixes (Evans, 2006). Injection mixes contained the selection marker pBX, which rescues *pha-1(e2123ts)* (Granato et al., 1994), and the Hygromycin resistance construct pIR98 (Radman et al., 2013), both at 50ng/µl. Mixes with GFP-expressing fosmids were injected into *unc-119(ed3) pha-1(e2123ts); arIs195* hermaphrodites. Mixes with Venus-expressing constructs were injected into *unc-119(ed3) pha-1(e2123ts); arIs198* hermaphrodites. Transformants were selected by *pha-1(ts)* rescue at 25°C. Thereafter transgenes were followed by fluorescent expression of constructs, *pha-1(ts)* rescue, and/or survival on hygromycin plates.

Table S2. Transgenes and plasmids

Transgene	Construct(s)	Plasmid	Concentration
arIs195	*glt-3p::LifeAct::TagRFP*	See Shaye and Greenwald, 2015	
arIs198	*glt-3*p::*CFP*		
	*glt-3*p::*LifeAct::TagRFP*		
arEx2348	*inft-2::gfp*	fosmid	25 ng/µl
arEx2349			
arEx2357	*cyk-1::gfp* fosmid	fosmid	25 ng/µl
arEx2358			
arEx2360	*glt-3*p::*Venus::exc-5*	pDS630	6 ng/µl
arEx2361			
arEx2404	*glt-3*p::*Venus*	pDS242	6 ng/µl
arEx2411			
arEx2405	*glt-3*p::*Venus::inft-2*	pDS453	6 ng/µl
arEx2406			
arEx2408	*glt-3*p::*Venus::cyk-1b*	pDS631	6 ng/µl
arEx2409			
arEx2410			

Note: all *glt-3*p-driven constructs use the *unc-54 3'UTR*.

Primers

For primers used to amplify cDNAs, blue sequences are heterologous, restriction sites used for cloning cDNAs into pDS242, the *glt-3*p::*Venus::unc-54*'3 vector, are underlined, start and stop codons are bold.

Table S3. Primers

Oligo	Sequence	Use
oDS320	ATGGATTTACCAGCGCAAAG	Detect *inft-2(ok1296)* allele deletion
oDS321	ATTCAACGGTCGAACAGAGC	
oDS322	CCGTTTTCTTCTGCTTCCTG	
oDS399	CGGGGTACCGACGTCAGGCGGCCGCGGACCGGTAAAA**ATG**GTGAAGAAGCGCCAAAAC	Amplify *inft-2* cDNA
oDS400	TCATCTAGAA**TCA**AACTGGACTTCCTACCAAGG	
oDS416	ACGAAGATGAACTTGTCGGC	Detect *cyk-1(ok2300)* allele deletion
oDS417	CAATGCAATGATGGAAGTCG	
oDS418	ACCGCTCTCAGCTTGTCAAT	

Primers (cont'd)

Oligo	Sequence	Use
oDS430	TCGTCTGATGATGATGGAC	Sequence *inft-2* cDNA
oDS431	TCCAAGACCATCCAACGGAG	
oDS432	ACATCCACTTCTCCCGTTC	
oDS501	TGCAAGTTGTTTGGTACGGA	Detect *cdc-42(gk388)* allele deletion
oDS502	CAAGAATGGGGTCTTTGAGC	
oDS503	ACGGCGTAATTGTCGAAGAC	
oDS646	AATGCCAGTGGAGAAGGAGC	Detect *cyk-1(or596ts)* allele. Use with oDS417
oDS694	CGGGGTACCCCCGGGCATAAAA**ATG**GAAGAACTCACGAAAACAGTTCGG	Amplify *exc-5* cDNA
oDS695	TCAACTAGTA**TTA**TACCGGTGCAGCTCCTTCAGATTGCTCGGATCCAGAATTCCG	
oDS696	TCCAGATTTGAGAAGTTCGC	Sequence *exc-5* cDNA
oDS697	TTACAAGCAGCTGCACATGC	
oDS703	CGGGATATCGGTACCCATAAAA**ATG**TCTAGCGATGATTATGAGTCAATTG	Amplify *cyk-1b* cDNA
oDS704	TCAGCGGCCGC**TCA**TGCTGAGCGGAAATCATTAAGACGTGCGAGAAG	
oDS705	GAGAATCATTTGCCTTGTCAGG	Sequence *cyk-1b* cDNA
oDS706	CAGTTATTGGCGGTAGAGC	

Spinning Disk Microscopy Settings

- INFT-2::GFP (Fig. 2B) grown at 25°C. GFP (488nm) laser power at 10.4%, EM gain 595, and exposure 360ms. TagRFP (561nm) laser power at 5.5%, EM gain 570, and exposure 150ms.
- Venus::INFT-2 (Fig. 2C, D) grown at 22°C. CFP (445nm) laser power at 1.0%, EM gain 650, and exposure 400ms. YFP (514nm) laser power at 15.0%, EM gain 605, and exposure 700ms. TagRFP (561nm) laser power at 10.0%, EM gain 600, exposure 700ms.
- CYK-1::GFP (Fig. 2E) grown at 25°C. GFP (488nm) laser power at 10.0%, EM gain 521, and exposure 600ms. TagRFP (561nm) laser power at 5.0%, EM gain 570, and exposure 260ms.
- Venus::CYK-1 (Fig. 2F) grown at 25°C. CFP (445nm) laser power at 1.0%, EM gain 650, and exposure 400ms. YFP (514nm) laser power at 14.4%, EM gain 605, and exposure 700ms. TagRFP (561nm) laser power at 10.0%, EM gain 685, exposure 685ms.
- Venus::INFT-2 (Fig. 4C, D) in *wild-type* subjected to temperature shift (15°C to 25°C) as control. CFP (445nm) laser power at 1.0%, EM gain 260, and exposure 400ms. YFP (514nm) laser power at 10.0%, EM gain 600, and exposure 650ms. TagRFP (561nm) laser power at 10.0%, EM gain 590, exposure 320ms.
- Venus::INFT-2 (Fig. 4C, D) in *cyk-1(ts)* subjected to temperature shift (15°C to 25°C) to reduce CYK-1 function. CFP (445nm) laser power at 1.0%, EM gain 260, and exposure 350ms. YFP (514nm) laser power at 10.0%, EM gain 600, and exposure 650ms. TagRFP (561nm) laser power at 3.0%, EM gain 590, exposure 400ms.

Supplementary References

Andersen, E. C., Saffer, A. M. and Horvitz, H. R. (2008). Multiple levels of redundant processes inhibit *Caenorhabditis elegans* vulval cell fates. *Genetics* **179**, 2001-2012.

Brenner, S. (1974). The genetics of *Caenorhabditis elegans*. *Genetics* **77**, 71-94.

Chalkia, D., Nikolaidis, N., Makalowski, W., Klein, J. and Nei, M. (2008). Origins and evolution of the formin multigene family that is involved in the formation of actin filaments. *Mol Biol Evol* **25**, 2717-2733.

Edgley, M. L., Baillie, D. L., Riddle, D. L. and Rose, A. M. (2006). Genetic balancers. *WormBook*.

Evans, T. C. (2006). Transformation and Microinjection. *WormBook*.

Granato, M., Schnabel, H. and Schnabel, R. (1994). *pha-1*, a selectable marker for gene transfer in *C. elegans*. *Nucleic Acids Research* **22**, 1762-1763.

Johnston, R. J., Jr., Copeland, J. W., Fasnacht, M., Etchberger, J. F., Liu, J., Honig, B. and Hobert, O. (2006). An unusual Zn-finger/FH2 domain protein controls a left/right asymmetric neuronal fate decision in *C. elegans*. *Development* **133**, 3317-3328.

Liu, R., Linardopoulou, E. V., Osborn, G. E. and Parkhurst, S. M. (2010). Formins in development: orchestrating body plan origami. *Biochim. Biophys. Acta* **1803**, 207-225.

Mi-Mi, L., Votra, S., Kemphues, K., Bretscher, A. and Pruyne, D. (2012). Z-line formins promote contractile lattice growth and maintenance in striated muscles of *C. elegans*. *J Cell Biol* **198**, 87-102.

Nezami, A. G., Poy, F. and Eck, M. J. (2006). Structure of the autoinhibitory switch in formin mDia1. *Structure* **14**, 257-263.

Radman, I., Greiss, S. and Chin, J. W. (2013). Efficient and rapid *C. elegans* transgenesis by bombardment and hygromycin B selection. *PLoS One* **8**, e76019.

Shaye, D. D. and Greenwald, I. (2015). The Disease-Associated Formin INF2/EXC-6 Organizes Lumen and Cell Outgrowth during Tubulogenesis by Regulating F-Actin and Microtubule Cytoskeletons. *Dev Cell* **32**, 743-755.

Sun, H., Schlondorff, J. S., Brown, E. J., Higgs, H. N. and Pollak, M. R. (2011). Rho activation of mDia formins is modulated by an interaction with inverted formin 2 (INF2). *Proc Natl Acad Sci USA* **108**, 2933-2938.